HHS Public Access

Author manuscript

Brain Stimul. Author manuscript; available in PMC 2023 September 27.

Published in final edited form as:

Brain Stimul. 2023 ; 16(4): 1196–1204. doi:10.1016/j.brs.2023.08.003.

Alteration of functional connectivity in the cortex and major brain networks of non-human primates following focused ultrasound exposure in the dorsal striatum

Dong Liu[a,b,*], **Fabian Munoz**[a,b], **Soroosh Sanatkhani**[a,b], **Antonios N. Pouliopoulos**[c], **Elisa E. Konofagou**[d,e], **Jack Grinband**[e,f], **Vincent P. Ferrera**[a,b,f]

[a]Department of Neuroscience, Columbia University, USA

[b]Zuckerman Mind Brain Behavior Institute, Columbia University, USA

[c]Department of Surgical & Interventional Engineering, School of Biomedical Engineering & Imaging Science, King's College London, UK

[d]Department of Biomedical Engineering, Columbia University, USA

[e]Department of Radiology, Columbia University, USA

[f]Department of Psychiatry, Columbia University, USA

Abstract

Background: Focused ultrasound (FUS) is a non-invasive neuromodulation technology that is being investigated for potential treatment of neurological and psychiatric disorders. FUS combined with microbubbles can temporarily open the intact blood-brain barrier (BBB) of animals and humans, and facilitate drug delivery. FUS exposure, either with or without microbubbles, has been demonstrated to alter the behavior of non-human primates (NHP), and previous studies have demonstrated the transient and long-term effects of FUS neuromodulation on functional connectivity using resting state functional MRI. The behavioral effects of FUS vary depending on whether or not it is applied in conjunction with microbubbles to open the BBB, but it is unknown whether opening the BBB affects functional connectivity differently than FUS alone.

Objective: To compare the effects of applying FUS alone (FUS neuromodulation) and FUS with microbubbles (FUS-BBB opening) on changes of resting state functional connectivity in NHP.

*Corresponding author. Jerome L. Greene Science Center, 3227 Broadway, Quad 6B, New York, NY, 10027, USA. dl3341@columbia.edu (D. Liu).

CRediT authorship contribution statement

Dong Liu: Formal analysis, Data curation, Conceptualization, Funding acquisition, Methodology, Writing – original draft, Writing – review & editing. **Fabian Munoz:** Formal analysis, Data curation, Writing – review & editing. **Soroosh Sanatkhani:** Formal analysis, Data curation. **Antonios N. Pouliopoulos:** Writing – review & editing. **Elisa E. Konofagou:** Funding acquisition, Writing – review & editing. **Jack Grinband:** Writing – review & editing. **Vincent P. Ferrera:** Conceptualization, Formal analysis, Writing – review & editing.

Declaration of competing interest

The authors declare that they have no known competing financial interests or personal relationships that could have appeared to influence the work reported in this paper.

Appendix A. Supplementary data

Supplementary data to this article can be found online at https://doi.org/10.1016/j.brs.2023.08.003.

Methods: We applied 2 min FUS exposure without (neuromodulation) and with microbubbles (BBB opening) in the dorsal striatum of lightly anesthetized non-human primates, and acquired resting state functional MRI 40 min respectively after FUS exposure. The functional connectivity (FC) in the cortex and major brain networks between the two approaches were measured and compared.

Results: When applying FUS exposure to the caudate nucleus of NHP, we found that both FUS neuromodulation can activate FC between caudate and insular cortex, while inhibiting the FC between caudate and motor cortex. FUS-BBB opening can activate FC between the caudate and medial prefrontal cortex, and within the frontotemporal network (FTN). We also found both FUS and FUS-BBB opening can significantly activate FC within the default mode network (DMN).

Conclusion: The results suggest applying FUS to a deep brain structure can alter functional connectivity in the DMN and FTN, and that FUS neuromodulation and FUS-mediated BBB opening can have different effects on patterns of functional connectivity.

Keywords

Focused ultrasound; Neuromodulation; Blood-brain barrier opening; Functional connectivity; Resting state functional MRI; Brain networks

1. Introduction

Focused ultrasound (FUS) is a non-invasive brain stimulation technology that is in early stages of translation to clinical applications in psychiatry and neurology. While high intensity focused ultrasound is capable of producing lesions [1,2], low intensity pulsed FUS can deliver repeated ultrasound bursts non-invasively into specific deep brain regions without trauma [3–6]. These properties make it an attractive alternative to other neuromodulation technologies, such as transcranial direct current stimulation (tDCS) [7] and transcranial magnetic stimulation (TMS) [8], both of which primarily target superficial brain regions. Animal studies have shown that FUS could be used for non-invasive cortical and subcortical brain stimulation with sub-millimeter focus [9], by inducing excitatory or inhibitory effects in the central or peripheral nervous system, depending on the pulsing regime [6]. FUS can also alter behavior in non-human primates (NHPs) [10–13].

The mechanism by which FUS can affect the functional connectivity of brain regions and networks has been studied using blood oxygenation level-dependent (BOLD) functional MRI (fMRI). Sanguinetti et al. found application of FUS to the prefrontal cortex can alter the functional connectivity and improve mood in humans [14]. In NHPs, recent studies used resting state fMRI to evaluate long-lasting or “offline” effects of FUS exposure on subcortical or deep cortical regions, including amygdala, anterior cingulate cortex [15], medial frontal cortex [16], and supplemental motor cortex [17]. Munoz et al. found that 2 min of FUS applied to the dorsal striatum can alter patterns of functional connectivity in the NHP brain that can last for hours and may be correlated with improvement in a cognitive task [12].

FUS combined with microbubbles has been used to reversibly per-meabilize the blood-brain barrier (BBB) and facilitate drug delivery both in animal and human studies [18,19], and

recent work has demonstrated that FUS exposure with microbubbles in the striatum can improve response speed and accuracy during visual-motor tasks in NHPs [20,21]. Using resting state fMRI, Todd et al. found that FUS-induced BBB opening can disrupt the functional connectivity between inter-hemispheric regions in rats [22]. Meng et al. found transient functional connectivity reductions with FUS BBB opening in the frontal lobe of patients with Parkinson's disease [23].

Although both FUS and FUS with microbubbles (BBB opening) have been shown to modulate neural activity, the impact of FUS-induced BBB opening on functional connectivity is not well understood. Changing the permeability of the BBB may alter blood perfusion, nutrient absorption, or tissue oxygenation near the BBB opening and may affect neural function differently than direct neuromodulation [24]. No prior studies have investigated the effects of FUS-mediated BBB opening on functional connectivity in non-human primates. Investigating how BBB opening differs from direct neuromodulation is needed to understand how BBB opening affects cognitive performance and to establish a baseline for evaluating the outcomes of FUS-mediated drug delivery in the treatment of neurological and psychiatric disorders. The objective of this study was to compare the effects of applying FUS (neuromodulation) and FUS combined with microbubbles (BBB opening) to the NHP dorsal striatum in order to determine how changes in resting state functional connectivity of major brain networks differs between the two approaches.

2. Results

2.1. Numerical simulation and post-FUS exposure confirmation

For precise targeting and energy deposition of FUS during the experiments, acoustic and biothermal simulations of a single element transducer (ROC = 64 mm) were conducted using Matlab k-Wave toolbox [25] and NHP skull CT (computer tomography) model. For burst mode ultrasound protocol described in Fig. 1A (500 kHz central frequency, 10 m s burst duration, 2 Hz pulse repetition frequency, 2% duty cycle and 2 min total sonication), both the peak negative pressure (PNP) and temperature distribution are shown in Fig. 1B. The PNP of the target at the right Caudate can reach above 800 kPa, while maximum temperature in the target is within 37.5 °C. More ultrasound energy was deposited in the skull due to its high absorption coefficients compared to soft brain tissue, and the temperature elevation reached 3–4 °C above baseline body temperature. Supplementary Fig. S1 demonstrates that the maximum temperature of the skull, muscle, and brain were 41.2 °C, 39.7 °C and 38.2 °C respectively, within the safety limits of the current guideline [26].

The planning and targeting of FUS exposure with and without microbubbles was achieved using the combined FUS and Brainsight neuro-navigation system. As shown in Fig. 2A, the FUS energy was delivered to target the region located in the caudate nucleus in the right hemisphere. To illustrate BBB opening sites due to FUS exposure, gadolinium enhanced structural scans were acquired in both baseline without FUS exposure and FUS with microbubbles (FUS-induced BBB opening). The subtraction image between the two gadolinium enhanced structural scans indicates the actual sites of FUS-BBB opening, as shown in the colored highlighted region of Fig. 2B. The BBB of the NHP brain was

successfully opened in the area of right caudate (Fig. 2B), with slight focus shifting compared with the planned target (green crossed point Fig. 2A).

2.2. Effects on the striatum and cortical regions

To quantify the functional connectivity due to FUS neuromodulation and BBB opening, a region of interest (ROI) with 3.5 × 3.5 × 3.5 mm^3 voxel at the right caudate was first chosen as a seed. The seed correlation maps of baseline, FUS, and FUS with microbubbles, as well as the difference maps are shown in Fig. 3, overlaid on the standard D99 NHP template [27]. With FUS exposure in the right caudate, the functional connectivity is found to be increased between caudate and insular cortex (IC: regions of Ial, Iapl and Id in both hemispheres shown in Fig. 4A), and between caudate and temporal cortex (areas RT, RTp and TGdd in both hemispheres shown in Fig. 4A) while the functional connectivity is reduced between caudate and motor cortex (MC: areas F1, F2, F3 and F4 in both hemispheres shown in Fig. 4A), and between caudate and so-matosensory cortex (SSC: areas 1, 2, 3a and 3b in both hemispheres shown in Fig. 4A). In contrast, when applying FUS with microbubbles, the alteration of functional connectivity does not show the similar pattern as above. Instead, a stronger activation of functional connectivity is found between caudate and medial prefrontal cortex (mPFC: areas 8Bm, 9m, 9d and 10mr in both hemispheres shown in Fig. 4A). Statistical analysis on representative regions (area 9m of mPFC; area Ial of IC and area F1 of MC) were performed, with results of both Kruskal-Wallis test and post-hoc permutation test are shown in Fig. 4B. With FUS exposure in the right caudate, the activation of insular cortex ($p < 0.001$ in right hemisphere and $p < 0.01$ in left hemisphere, compared to baseline and FUS-BBB opening) and inhibition of the motor cortex ($p < 0.001$ in both hemispheres, compared to other two conditions) is statistically significant, while with FUS-mediated BBB opening, significant changes of functional connectivity is only found within mPFC ($p < 0.01$ compared to baseline).

2.3. Effects on the default mode network

To quantify the effect of FUS on the default mode network, an ROI of 3.5 × 3.5 × 3.5 mm^3 voxel was placed in the area 8Ad of dlPFC within the default mode network (DMN), with the central coordinates of the ROI listing in Supplementary Table S1. The average correlation maps of baseline, FUS and FUS BBB opening, as well as the difference maps were calculated with the results shown in Fig. 5B. Both FUS and FUS with microbubbles demonstrate an activation of the default mode network (DMN) (Fig. 5A and B), a network connecting dorsolateral prefrontal cortex (dlPFC), posterior cingulate cortex (PCC) and posterior parietal cortex (PPC) of NHPs. The average correlations with FUS BBB opening within the DMN nodes is greater than the correlations with FUS only (Fig. 5C). Statistical analysis on representative nodes (area 8Ad in dlPFC, areas 31 and 23b in PCC and areas LIPd in PPC, area TPO in temporal lobe (TEMP)) was performed, with the results of Kruskal-Wallis test for comparison among the three conditions, and post-hoc permutation test for comparison between each two conditions, as shown in Fig. 6A. With either FUS or FUS combined with microbubbles, significant functional connectivity changes were found between dlPFC and the areas of PPC, PPC and TEMP. When placing the seed at area 23b of PCC, the connectivity between PCC and dlPFC was also found to be significantly enhanced (Fig. 6C) at these two conditions. However, the functional connectivity due to FUS and

FUS with microbubbles was not significantly different (post-hoc permutation test: $p > 0.05$, shown in Fig. 6A).

2.4. Effects on the frontotemporal network and other networks

The effects of FUS neuromodulation and BBB opening on the frontotemporal network of the NHP, which connects the areas of mPFC and the temporal lobe, were evaluated. When selecting area 9m as a seed ROI in mPFC, only FUS combined with microbubbles demonstrates significant activation of functional connectivity between mPFC and regions of TEMP and PCC, as shown in, Supplementary Fig. S2 and Fig. 6B while FUS (without microbubbles) failed to alter the functional connectivity significantly between mPFC and TEMP, compared to the baseline (FUS vs Baseline via post-hoc permutation test: $p > 0.05$, shown in Fig. 6B).

While significant alteration of functional connectivity within DMN and FTN is found, the effect of FUS on other brain networks is not conclusive. For example, with the seed ROI of Ial, the average correlation between insular cortex and anterior cingulate cortex (ACC) with FUS-induced BBB opening is slightly higher than the correlations with the other two conditions, however, no statistically significant difference is found between FUS and FUS with microbubbles (Permutation test, $p > 0.05$, shown in Fig. 6D). With the seed ROI chosen as primary visual cortex, no clear alteration of the functional connectivity is found between visual cortex and the other brain regions (Supplementary Fig. S3), and no statistical difference is found among baseline, FUS and FUS with microbubbles (Kruskal-Wallis test, $p > 0.05$, shown in Fig. 6E).

3. Discussion

By comparing the “offline” resting state functional connectivity after applying 2 min FUS exposure with and without microbubbles in dorsal striatum of nonhuman primates, we found that FUS neuromodulation and FUS BBB opening affect patterns of functional connectivity differently. FUS neuromodulation can increase functional connectivity between caudate and insular cortex and decrease functional connectivity between caudate and motor cortex, while FUS-mediated BBB opening can increase functional connectivity between caudate and medial prefrontal cortex and the nodes within the frontotemporal network (Fig. 7B). The findings provide further evidence that FUS can be used as a neuromodulation technology to selectively modulate cortical and subcortical brain regions, which are commensurate with other studies [11,15,28]. Specifically, alteration of functional connectivity between the caudate and cortical regions is comparable in magnitude with the previous studies, and we used relatively lower average ultrasound intensity and slightly longer sonication compared to the other neuromodulation studies [11,15,28]. It is likely that different parameters including pressure, burst duration, duty cycle, pulse repetition frequency may have varying effects on functional connectivity of NHPs and further FUS neuromodulation investigations involving these parameters should be performed in the future studies.

In this study, we measured the functional connectivity after FUS exposure combined with microbubbles. The current FUS protocol (400 kPa derated PNP, 2% duty cycle, 2 Hz PRF and 2 min sonication) combined with circulating microbubbles for BBB opening has

a mechanical index of 0.56, within the FDA limit of 0.8 for using circulating Definity microbubbles in imaging applications. While higher PNP may be explored to increase BBB opening volume, unstable microbubble cavitation may be generated if the mechanical index exceeds the FDA limit [29]. The safety of the current FUS-induced BBB opening protocol with 400 kPa derated PNP has been validated through multiple previous works on NHPs, with no report of hemorrhage or edema [29,30]. Even though microbubbles were proved to enhance the HIFU thermal therapy, one previous study found very slight temperature elevation (<0.1 °C) when applying extremely low duty cycle (2%) FUS combined with microbubbles [30].

Similar to recent findings in rodents [22] and humans [23], the current study found that FUS-mediated BBB opening can alter functional connectivity in NHP. The substantial difference of the resting state fMRI results between FUS and FUS-induced BBB opening with the same derated PNP (400 kPa) implied that FUS combined with microbubbles might be the driving force for changes of functional connectivity (Supplementary Fig. S4). Currently, FUS-mediated BBB opening for drug delivery has demonstrated promising results in clinical trials, our study suggests that an accompanying neuromodulation effect may occur during the procedure of FUS-mediated BBB opening. Different patterns of functional connectivity suggest that direct FUS and FUS BBB opening have different neuromodulation effects. This finding also reflects the results in visual-motor tasks in NHPs after applying FUS exposure with and without microbubbles: NHP improved accuracy along with a shorter response time after applying FUS exposure combined with microbubbles [21,29], suggesting increased decision efficiency, while NHP showed more accuracy but with a longer response time after applying FUS exposure only, consistent with a speed-accuracy trade-off [12]. One possible explanation of the difference between FUS neuromodulation and FUS-induced BBB opening is that when BBB is opened by FUS combined with microbubbles in the target region, the blood oxygenation and water perfusion in that region may change as well [24]. This may underlie changes in BOLD activation for resting state functional MRI. Future studies plan to address quantitative measurement of the blood oxygenation of FUS and FUS BBB opening using advanced MRI.

The study also demonstrated that applying FUS exposure in the caudate nucleus could activate the default mode network on lightly anesthetized NHP (Fig. 7A). Similar trends were found between FUS and FUS BBB opening, however we could not significantly differentiate the magnitude of functional connectivity of the two due to limited NHP experiments in this study. Findings from both FUS neuromodulation and FUS-mediated BBB opening may improve our understanding of the role of striatum in regulating cortical circuits, as well as the functional connection between striatum and default mode network. While the mechanism for external FUS stimulation in modulating the DMN via striatum is still unknown, one possible explanation may suggest striatum may “communicate” with cortical regions within DMN in a similar way with thalamus, which can both drive and modulate cortical regions [31]. A recent study in humans found that a reward task can enhance the connection between existing DMN and ventral striatum [32], which also supports the idea that the striatum may play a role in regulating the DMN.

This study has several limitations. Firstly, awake and anesthetized NHP may have different patterns of functional connectivity [33], and isoflurane may affect the results of functional connectivity [34], although in this study we used a well-established NHP anesthesia protocol [35] with similar concentration (~1.0%) isoflurane as the other NHP rsfMRI studies. Functional connectivity was also reported to be related with age [36], and in this study, one NHP involved in the FUS neuromodulation study is much older (~27 years old) than the other NHPs. We could not rule out the effect of age on the results due to limited NHP resources. Another aspect that may affect variation of functional connectivity is the seed ROI we selected in this study [37]. For example, when evaluating the effect of FUS on DMN, we selected some representative ROI's in DMN following recent work evaluating DMN among primates [38]. Since the organization of DMN varies among non-human primates and humans [39], we tested different seeds (i.e. areas 8Ad, 46d, 8Bs in dlPFC, shown in Supplementary Fig. S5) in this study to make sure the results are valid and robust.

In conclusion, this study compared the resting state functional connectivity on NHP after FUS neuromodulation and FUS-mediated BBB opening and found different alteration patterns in various cortical regions. Applying FUS to deep brain structures can alter functional connectivity in major brain networks such as the default mode network and frontotemporal network.

4. Materials and methods

4.1. Animal preparation

A total of six adult male NHPs (N, P, O, Q, M and T, 6.9–12.3 kg, 10–27 years old) were used in the experiments. Two NHPs (P and O) were selected to apply FUS exposure only and two NHPs (M and T) were selected to apply FUS exposure with microbubbles. All the six NHPs were scanned to acquire structural and functional MRI images. Prior to the ultrasound and MRI experiments, all the NHPs were firstly sedated with ketamine (10 mg/kg) and dexmedetomidine (0.02 mg/kg) and then were anesthetized with 0.8–1.5% isoflurane. The head skin of each NHP was shaved and the conductive gel was applied to achieve optimal ultrasound sonication. During the MRI experiments, the Iradimed 3880 MRI compatible monitoring system (Winter Springs, FL, USA) was used to wirelessly monitor the vital signs of NHPs including body temperature, electrocardiogram, oxygen saturation and respiratory CO2. All the NHP procedures were approved by the Institutional Animal Care and Use Committee (IACUC) of Columbia University.

4.2. FUS neuromodulation and BBB opening

A single element FUS transducer (H-107, 500 kHz frequency, 63.2 mm radius of curvature (ROC), 64 mm outer diameter (OD), Sonic Concepts, Bothell, WA) was driven by a functional generator (Aglient 33220 A, Agilent Technologies, Santa Clara, CA) connecting to a 57 dB radiofrequency power amplifier (500S06, E&I, Rochester, NY). The FUS transducer was calibrated at a tank filled with degassed water. The free field pressure, the acoustic focus and acoustic intensities (including Isppa: spatial-peak pulse average, and Ispta: spatial-peak temporal average) were measured using a capsule hydrophone (HGL-0200, Onda Corp. Sunnyvale, CA). To better estimate the actual acoustic pressure

at the focus region, we measured the attenuation of the acoustic pressure through two ex-vivo NHP skulls. At the calibrated free field pressure range (200 kPa–1600 kPa), the average attenuation of the pressure was measured as 47.3 ± 3.3%. The transcranial PNP that considered pressure loss due to the skull attenuation, was referred to as derated PNP in the result section.

On the same day of MRI session, the transducer cone was filled with degassed water using a water degassing system WDS105+ (Sonic Concepts, Bothell, WA), and was inflated to attach the scalp for efficiently delivering ultrasound energy to the target. A FUS protocol described in previous studies [12,40] was adopted in order to achieve safe and efficient neuromodulation and BBB opening on NHPs, with detailed sonication parameters shown in Fig. 1A. For the group with FUS neuromodulation, FUS generated by the single element FUS transducer was applied on NHPs O and P for 2 min with derated PNP of 800 kPa, 2 Hz pulse repetition frequency (PRF), 10 m s pulse duration (PD) and 2% duty cycle. For the group with FUS-BBB opening, same FUS parameters but with derated PNP of 400 kPa were applied on NHPs M and T, and in-house manufactured microbubbles (MB) (4–5 μm diameter, 2.5 $\times 10^8$ bubbles/kg) was injected intravenously through the saphenous vein of NHPs 10s after starting of the ultrasound sonication. The spatial peak temporal average intensities (Ispta) of the FUS neuromodulation and FUS-BBB opening are 156.9 mW/cm^2 and 39.2 mW/cm^2 respectively. In this way, a lower ultrasound intensity was used to eliminate the effects of neuromodulation but efficiently and safely enough to open the intact BBB of NHP, as reported in the previous literature [29].

4.3. Targeting and numerical simulation

To achieve precise targeting of each NHP, a real time neuro-navigation system (BrainSight Vet System, Rogue Research Inc. Canada) in conjunction with the ultrasound system described in previous works was used [41]. After calibrating the FUS transducer in water at room temperature, we set up a numerical model incorporating a FUS transducer (ROC = 64 mm) adopted in this study and an NHP CT model, and both 3D acoustic and biothermal simulations were performed in Matlab k-wave toolbox [25]. For all the tissues including skull, brain and muscle, speed of sound and the density were set up following a linear relation with CT Hounsfield units [42], frequency dependent attenuation coefficients were adopted based on previous measurement [43,44]. The detailed acoustic and thermal parameters for numerical simulation were listed in Supplementary Table S2 [45]. The initial temperature of the tissue was set as 37 °C. To prevent the skull from heating, the cone water temperature was set as 22 °C to provide further protection to the surface of the skull including before and immediately after FUS procedures. To simulate the actual scenario, 1-min pre-cooling and 2 min post cooling was incorporated in the k-wave thermal simulation. Temporal temperature evaluation of the brain, skull, and the other tissue were calculated based on Pennes Bioheat Equation [46]. Both acoustic pressure and temperature distribution on the 3D numerical model were finally acquired to evaluate the targeting accuracy and thermal safety.

4.4. MRI imaging

All the NHPs were placed on an MRI compatible stereotaxic device for MRI imaging at 3 T Siemens scanner, and an 8-channel surface receiver array coil was used to acquire both structural and functional MRI images. Under 0.8–1.1% light anesthesia, the resting state functional MRI scans were performed on NHPs (M, N, O, P, Q, T) using a T2* weighted EPI sequence (TR = 2000 m s; TE = 28.2 m s; FA = 70°; 1.65 mm isotropic resolution, FOV = 106 × 106 × 53 mm^3, 64 × 64 × 32 matrix voxels, 456 vol per run). The baseline scans were performed including 2–4 runs (~15 min per run, shown in Fig. 1A) per session for a total of 6 NHPs and 18 runs, but without FUS sonication. For the groups of NHPs undergoing FUS neuromodulation (NHPs O and P) and FUS BBB opening (NHPs M and T), a continuous 4 runs of resting state fMRI were acquired in one MRI session starting at approximately 45 min after 2 min FUS exposure described in the previous section. A total of 8 runs of resting state fMRI were acquired in the groups of FUS neuromodulation and FUS-induced BBB opening. In the same session of the functional scans, the T1 weighted structural scans were also acquired (TR = 2580 m s; TE = 2.81 m s; FA = 9°, isotropic 0.5 mm resolution; FOV 128 × 128 × 60 mm).

To evaluate the safety and efficiency of BBB opening, additional T1 weighted structural scans (same protocol with the regular T1, named post T1 in Fig. 1A) without (baseline + Gadolinium) and with FUS combined with microbubbles (FUS + Gadolinium + MB) were acquired 30 min after IV administration of Gadolinium contrast agent (0.2 ml/kg). In normal condition, the Gadolinium contrast cannot cross the intact BBB due to its relatively large molecular size, however with FUS-mediated BBB opening, the contrast agent was utilized as an efficient means to visualize the site of BBB opening due to its increasing effects on BBB permeability [40].

4.5. Data processing and analysis

All the fMRI data were processed using a pipeline combining FSL (FSL 6.0.3) and Matlab (Matlab 2019b, The MathWorks, Inc., Natick, MA, United States). First, preprocessing steps including motion correction, slice-timer correlation and B0 field map distortion correction were applied using FSL 6.0.3 [47]. Both temporal and spatial filtering were applied: a high pass temporal filter with 100 s cutoff was applied to remove the low-frequency noise; and a spatial filter with 3 mm FWHM Gaussian kernel was applied to smooth the fMRI data. In addition, global signal regression was applied on each dataset to remove the global artifacts due to motion and respiration [48,49]. Finally, linear registration was achieved from functional to structural images, and then from structural images to the standard D99 template of NHP brain [27], using the FAST tools of FSL [47].

In order to calculate the functional connectivity of the NHPs, we calculated seed-based correlation between the chosen ROI of 3.5 × 3.5 × 3.5 mm^3 and the other nodes or areas within the relevant brain networks including default mode network (DMN), frontotemporal network (FTN), salience network (SN) and visual networks (VN). For quantification of functional connectivity in cortical regions, we selected ROI located at right Caudate; for quantification of different brain networks, we selected ROI located at dorsolateral prefrontal cortex (DMN)), medial prefrontal cortex (FTN), insular cortex (SN) and primary visual

cortex (VN). The central coordinates of the ROI adopted in this study are listed in Table S1. The procedures above are performed for every run of resting state fMRI of NHPs including 18 baseline runs (6 sessions and 6 NHPs), 8 runs of FUS neuromodulation (2 sessions and 2 NHPs) and 8 runs of FUS-mediated BBB opening (2 sessions and 2 NHPs). In each run of the rsfMRI acquisition, the correlation coefficients between the seed ROI and the other brain area were calculated and the results were presented using Fisher'Z transformation. The resulting average correlations of all the rsfMRI runs in each group were then fed into Kruskal-Wallis test [50] to compare the BOLD activity between baseline, FUS neuromodulation and FUS-mediated BBB opening. The statistical threshold was set as 0.05, and when there is a statistical significant difference between the three groups, a post-hoc non parametric permutation test [51] with 5000 resamples were performed to compare the correlations between every two groups, with $p < 0.05$ representing a significance difference.

Supplementary Material

Refer to Web version on PubMed Central for supplementary material.

Acknowledgements

The authors wish to acknowledge the ZI-ICM team for the experiential setup and anesthesia procedures during MRI imaging, and Dr. Ray F. Lee for MRI sequence setup and data collection. The work is supported by NIH R01-MH112142, R01-MH133020, and DAPRA contract N 66001-19-C-4020 to V.P.F., NIH R01-EB009041 and R01-AG038961 to E.E.K., and BBRF Young Investigator Grant 31298 to D.L.

References

[1]. Ter Haar G, Coussios C. High intensity focused ultrasound: past, present and future. Int J Hyperther 2007;23(2):85–7.

[2]. McDannold N, Clement GT, Black P, Jolesz F, Hynynen K. Transcranial magnetic resonance imaging–guided focused ultrasound surgery of brain tumors: initial findings in 3 patients. Neurosurgery 2010;66(2):323–32. [PubMed: 20087132]

[3]. Kubanek J Neuromodulation with transcranial focused ultrasound. Neurosurg Focus 2018;44(2):E14.

[4]. Munoz F, Aurup C, Konofagou EE, Ferrera VP. Modulation of brain function and behavior by focused ultrasound. Curr Behav Neurosci Rep 2018;5(2):153–64. [PubMed: 30393592]

[5]. Kamimura HA, Conti A, Toschi N, Konofagou EE. Ultrasound neuromodulation: mechanisms and the potential of multimodal stimulation for neuronal function assessment. Frontiers in physics 2020;8:150. [PubMed: 32509757]

[6]. Blackmore J, Shrivastava S, Sallet J, Butler CR, Cleveland RO. Ultrasound neuromodulation: a review of results, mechanisms and safety. Ultrasound Med Biol 2019;45(7):1509–36. [PubMed: 31109842]

[7]. Nitsche MA, Cohen LG, Wassermann EM, Priori A, Lang N, Antal A, et al. Transcranial direct current stimulation: state of the art 2008. Brain Stimul 2008;1 (3):206–23. [PubMed: 20633386]

[8]. Walsh V, Cowey A. Transcranial magnetic stimulation and cognitive neuroscience. Nat Rev Neurosci 2000;1(1):73–80. [PubMed: 11252771]

[9]. Tufail Y, Matyushov A, Baldwin N, Tauchmann ML, Georges J, Yoshihiro A, et al. Transcranial pulsed ultrasound stimulates intact brain circuits. Neuron 2010;66(5): 681–94. [PubMed: 20547127]

[10]. Deffieux T, Younan Y, Wattiez N, Tanter M, Pouget P, Aubry J-F. Low-intensity focused ultrasound modulates monkey visuomotor behavior. Curr Biol 2013;23 (23):2430–3. [PubMed: 24239121]

[11]. Fouragnan EF, Chau BKH, Folloni D, Kolling N, Verhagen L, Klein-Flugge M, et al. The macaque anterior cingulate cortex translates counterfactual choice value into actual behavioral change. Nat Neurosci 2019;22(5):797–808. [PubMed: 30988525]

[12]. Munoz F, Meaney A, Gross A, Liu K, Pouliopoulos A, Liu D, et al. Long term study of motivational and cognitive effects of low-intensity focused ultrasound neuromodulation in the dorsal striatum of nonhuman primates. Brain Stimul 2022; 15(2):360–72. [PubMed: 35092823]

[13]. Banaie Boroujeni K, Sigona MK, Treuting RL, Manuel TJ, Caskey CF, Womelsdorf T. Anterior cingulate cortex causally supports flexible learning under motivationally challenging and cognitively demanding conditions. PLoS Biol 2022;20(9): e3001785. [PubMed: 36067198]

[14]. Sanguinetti JL, Hameroff S, Smith EE, Sato T, Daft CMW, Tyler WJ, et al. Transcranial focused ultrasound to the right prefrontal cortex improves mood and alters functional connectivity in humans. Front Hum Neurosci 2020;14:52. [PubMed: 32184714]

[15]. Folloni D, Verhagen L, Mars RB, Fouragnan E, Constans C, Aubry JF, et al. Manipulation of subcortical and deep cortical activity in the primate brain using transcranial focused ultrasound stimulation. Neuron 2019;101(6):1109–11016 e5. [PubMed: 30765166]

[16]. Bongioanni A, Folloni D, Verhagen L, Sallet J, Klein-Flügge MC, Rushworth MF. Activation and disruption of a neural mechanism for novel choice in monkeys. Nature 2021;591(7849):270–4. [PubMed: 33408410]

[17]. Verhagen L, Gallea C, Folloni D, Constans C, Jensen DE, Ahnine H, et al. Offline impact of transcranial focused ultrasound on cortical activation in primates. Elife 2019;8.

[18]. McDannold N, Arvanitis CD, Vykhodtseva N, Livingstone MS. Temporary disruption of the blood-brain barrier by use of ultrasound and microbubbles: safety and efficacy evaluation in rhesus macaques. Cancer Res 2012;72(14):3652–63. [PubMed: 22552291]

[19]. Meng Y, Pople CB, Lea-Banks H, Abrahao A, Davidson B, Suppiah S, et al. Safety and efficacy of focused ultrasound induced blood-brain barrier opening, an integrative review of animal and human studies. J Contr Release 2019;309:25–36.

[20]. Chu PC, Liu HL, Lai HY, Lin CY, Tsai HC, Pei YC. Neuromodulation accompanying focused ultrasound-induced blood-brain barrier opening. Sci Rep 2015;5:15477. [PubMed: 26490653]

[21]. Downs ME, Teichert T, Buch A, Karakatsani ME, Sierra C, Chen S, et al. Toward a cognitive neural prosthesis using focused ultrasound. Front Neurosci 2017;11:607. [PubMed: 29187808]

[22]. Todd N, Zhang Y, Arcaro M, Becerra L, Borsook D, Livingstone M, et al. Focused ultrasound induced opening of the blood-brain barrier disrupts inter-hemispheric resting state functional connectivity in the rat brain. Neuroimage 2018;178: 414–22. [PubMed: 29852281]

[23]. Meng Y, MacIntosh BJ, Shirzadi Z, Kiss A, Bethune A, Heyn C, et al. Resting state functional connectivity changes after MR-guided focused ultrasound mediated blood-brain barrier opening in patients with Alzheimer's disease. Neuroimage 2019;200:275–80. [PubMed: 31254646]

[24]. Todd N, Zhang Y, Livingstone M, Borsook D, McDannold N. The neurovascular response is attenuated by focused ultrasound-mediated disruption of the blood-brain barrier. Neuroimage 2019;201:116010. [PubMed: 31302253]

[25]. Treeby BE, Cox BT, Wave k-. MATLAB toolbox for the simulation and reconstruction of photoacoustic wave fields. J Biomed Opt 2010 Mar-Apr;15(2): 021314. 10.1117/1.3360308. [PubMed: 20459236]

[26]. Moyano DB, Paraiso DA, González-Lezcano RA. Possible effects on health of ultrasound exposure, risk factors in the work environment and occupational safety review. Health Care 2022 Feb 24;10(3):423. 10.3390/healthcare10030423.

[27]. Reveley C, Gruslys A, Ye FQ, Glen D, Samaha J, Er B, et al. Three-dimensional digital template atlas of the macaque brain. Cerebr Cortex 2017;27(9):4463–77.

[28]. Verhagen L, Gallea C, Folloni D, Constans C, Jensen DE, Ahnine H, et al. Offline impact of transcranial focused ultrasound on cortical activation in primates. Elife 2019;8:e40541. [PubMed: 30747105]

[29]. Pouliopoulos AN, Kwon N, Jensen G, Meaney A, Niimi Y, Burgess MT, et al. Safety evaluation of a clinical focused ultrasound system for neuronavigation guided blood-brain barrier opening in non-human primates. Sci Rep 2021;11(1):1–17. [PubMed: 33414495]

[30]. Pouliopoulos AN, Wu SY, Burgess MT, Karakatsani ME, Kamimura HA, Konofagou EE. A clinical system for non-invasive blood–brain barrier opening using a neuronavigation-guided single-element focused ultrasound transducer. Ultrasound Med Biol 2020 Jan 1;46(1):73–89. [PubMed: 31668690]

[31]. Sherman SM. Thalamus plays a central role in ongoing cortical functioning. Nat Neurosci 2016;19(4):533–41. [PubMed: 27021938]

[32]. Dobryakova E, Smith DV. Reward enhances connectivity between the ventral striatum and the default mode network. Neuroimage 2022;258:119398. [PubMed: 35724856]

[33]. Xu T, Sturgeon D, Ramirez JS, Froudist-Walsh S, Margulies DS, Schroeder CE, et al. Interindividual variability of functional connectivity in awake and anesthetized rhesus macaque monkeys. Biol Psychiatr: Cognitive Neuroscience and Neuroimaging 2019;4(6):543–53.

[34]. Zhang Z, Cai D-C, Wang Z, Zeljic K, Wang Z, Wang Y. Isoflurane-induced burst suppression increases intrinsic functional connectivity of the monkey brain. Front Neurosci 2019;13:296. [PubMed: 31031580]

[35]. Zhang X Effects of anesthesia on cerebral blood flow and functional connectivity of nonhuman primates. Veterinary Sciences 2022;9(10):516. [PubMed: 36288129]

[36]. Rao B, Xu D, Zhao C, Wang S, Li X, Sun W, et al. Development of functional connectivity within and among the resting-state networks in anesthetized rhesus monkeys. Neuroimage 2021;242:118473. [PubMed: 34390876]

[37]. Lv H, Wang Z, Tong E, Williams LM, Zaharchuk G, Zeineh M, et al. Resting-state functional MRI: everything that nonexperts have always wanted to know. Am J Neuroradiol 2018;39(8):1390–9. [PubMed: 29348136]

[38]. Mantini D, Gerits A, Nelissen K, Durand J-B, Joly O, Simone L, et al. Default mode of brain function in monkeys. J Neurosci 2011;31(36):12954–62. [PubMed: 21900574]

[39]. Garin CM, Hori Y, Everling S, Whitlow CT, Calabro FJ, Luna B, et al. An evolutionary gap in primate default mode network organization. Cell Rep 2022;39 (2):110669. [PubMed: 35417698]

[40]. Karakatsani MEM, Samiotaki GM, Downs ME, Ferrera VP, Konofagou EE. Targeting effects on the volume of the focused ultrasound-induced blood-brain barrier opening in nonhuman primates in vivo. IEEE Trans Ultrason Ferroelectrics Freq Control 2017;64(5):798–810.

[41]. Wu SY, Aurup C, Sanchez CS, Grondin J, Zheng W, Kamimura H, et al. Efficient blood-brain barrier opening in primates with neuronavigation-guided ultrasound and real-time acoustic mapping. Sci Rep 2018;8(1):7978. [PubMed: 29789530]

[42]. Deffieux T, Konofagou EE. Numerical study of a simple transcranial focused ultrasound system applied to blood-brain barrier opening. IEEE Trans Ultrason Ferroelectrics Freq Control 2010;57(12):2637–53.

[43]. Goss S, Frizzell L, Dunn F. Ultrasonic absorption and attenuation in mammalian tissues. Ultrasound Med Biol 1979;5(2):181–6. [PubMed: 556199]

[44]. Pinton G, Aubry JF, Bossy E, Muller M, Pernot M, Tanter M. Attenuation, scattering, and absorption of ultrasound in the skull bone. Med Phys (Woodbury) 2012;39(1):299–307.

[45]. Duck FA. Physical properties of tissues: a comprehensive reference book. Academic press; 2013.

[46]. Pennes HH. Analysis of tissue and arterial blood temperatures in the resting human forearm. J Appl Physiol 1948;1(2):93–122. [PubMed: 18887578]

[47]. Jenkinson M, Beckmann CF, Behrens TE, Woolrich MW, Smith SM. Fsl. Neuroimage 2012;62(2):782–90. [PubMed: 21979382]

[48]. Murphy K, Fox MD. Towards a consensus regarding global signal regression for resting state functional connectivity MRI. Neuroimage 2017;154:169–73. [PubMed: 27888059]

[49]. Wong CW, Olafsson V, Tal O, Liu TT. The amplitude of the resting-state fMRI global signal is related to EEG vigilance measures. Neuroimage 2013;83:983–90. [PubMed: 23899724]

[50]. McKight PE, Najab J. Kruskal-wallis test. The corsini encyclopedia of psychology. 2010. 1–1.

[51]. Nichols TE, Holmes AP. Nonparametric permutation tests for functional neuroimaging: a primer with examples. Hum Brain Mapp 2002;15(1):1–25. [PubMed: 11747097]

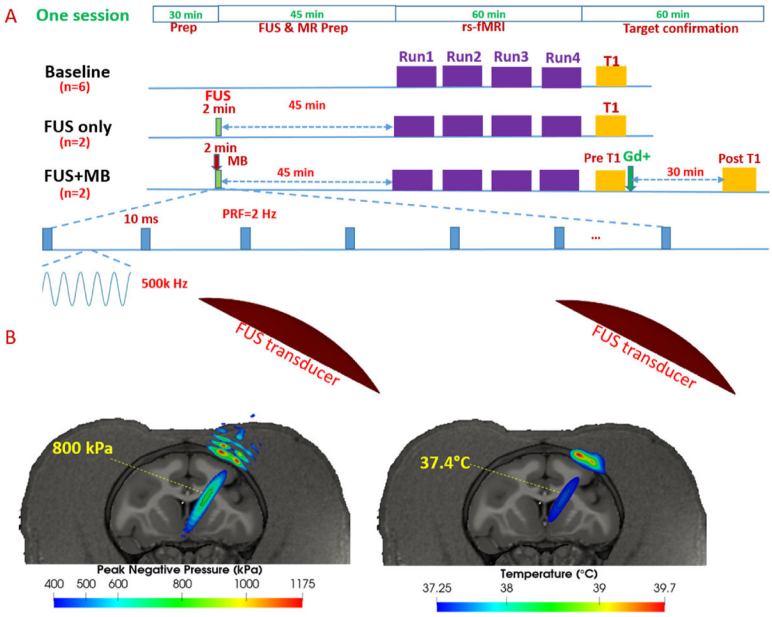

Fig. 1.

MRI and FUS experimental setup and numerical simulation A. MRI and FUS scheme of single session including baseline (n = 6 NHPs), FUS (FUS only, n = 2 NHPs) and FUS with microbubbles (FUS + MB, n = 2 NHPs); B. FUS Acoustic (derated PNP ~800 kPa in the target, used for FUS neuromodulation) and biothermal simulation (~0.5 °C elevation in the target).

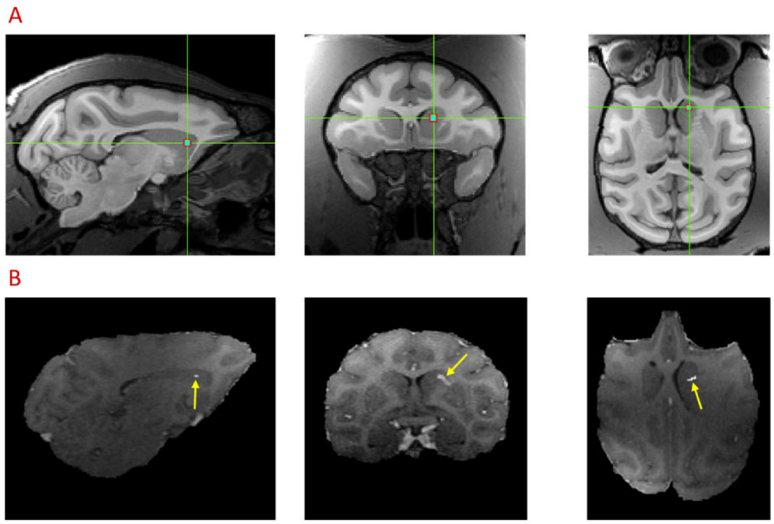

Fig. 2.

FUS target planning (A) and confirmation (B) using Gadolinium enhanced MRI images in sagittal, coronal and axial planes. The green-crossed point indicates the pre-treatment target of FUS exposure using Brainsight Navigation System (A). The hyper-intense voxels (yellow arrow) denote the region of BBB opening (B). Subtraction between Gadolinium enhanced T1 images collected at post FUS + MB and baseline was performed, and the difference in target area was shown with an overlay on post Gadolinium T1 images after FUS-induced BBB opening.

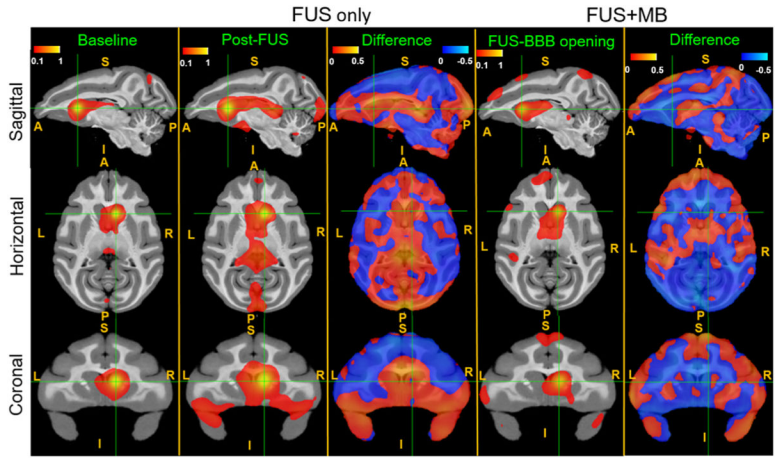

Fig. 3.

Effects of FUS and FUS-BBB opening on the functional connectivity between the caudate and the cortex. Seed-based connectivity and difference maps of resting state fMRI without FUS (baseline), post-FUS (FUS only) and post-FUS with microbubbles (FUS + MB). Connectivity changes were found in the after FUS and FUS-BBB opening compared to the baseline. The red-yellow and blue-light blue color maps indicate Fisher z-score maps with seeds in the right caudate (FUS target, shown in green cross point). L: left, R: right, A: anterior, P: posterior, S: superior, I: inferior.

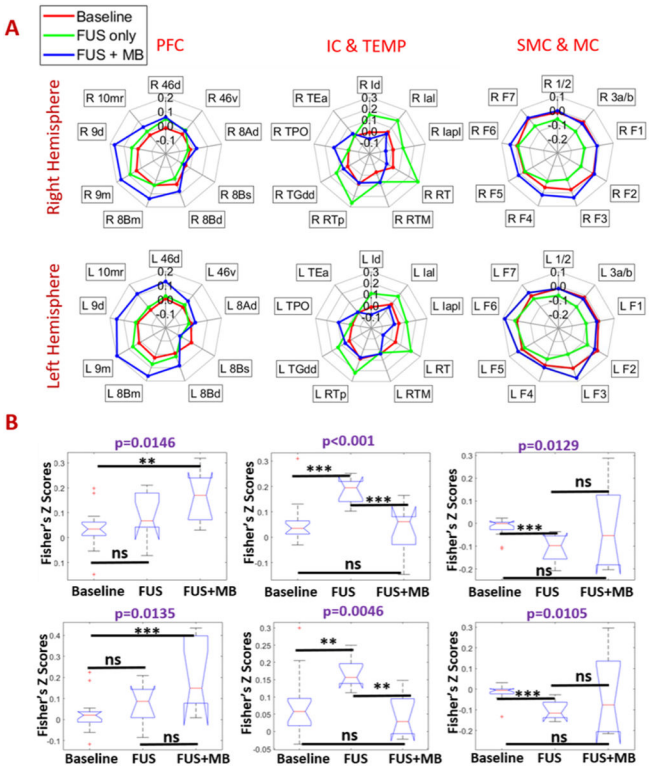

Fig. 4.

Effects of FUS and FUS-BBB opening on the functional connectivity between the caudate and the cortex: radar charts (A) and statistical box plots (B) of resting state fMRI without FUS (baseline), post-FUS (FUS only) and post-FUS with microbubbles (FUS + MB). The box plots showed the correlations of 25% percentile, 50% percentile, and 75% percentile, and outlining or extremely values. Statistical analysis was firstly performed using Kruskal-wallis test, with a purple $p < 0.05$ representing a significant difference. Post-hoc permutation test (5000 resamples) was performed to compare correlation values between each pair of three conditions. When there is a significant difference among the three conditions, and × denotes $p < 0.05$, ** denotes $p < 0.01$, *** denotes $p < 0.001$ and ns denotes $p > 0.05$.

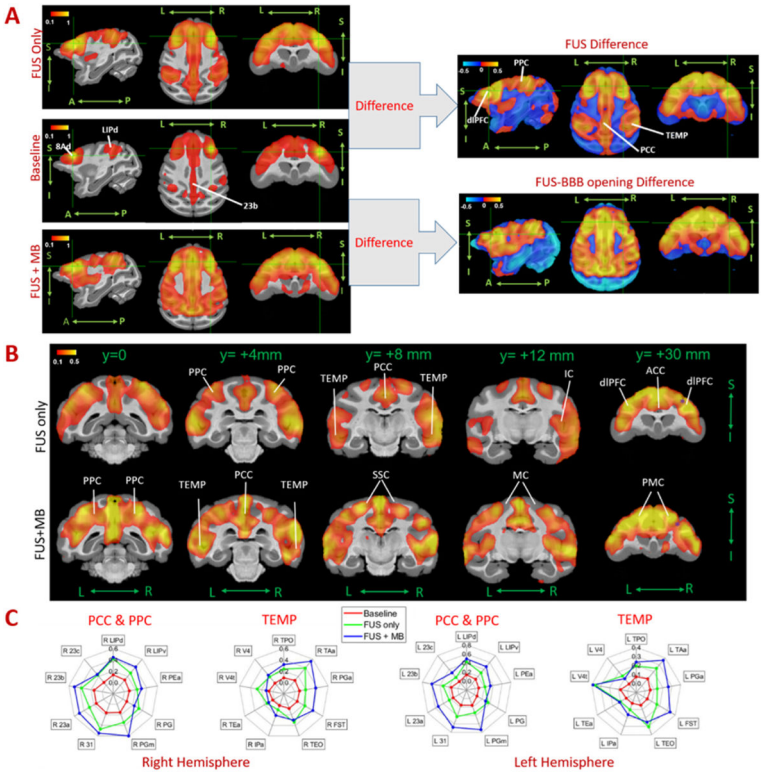

Fig. 5.

Effects of FUS and FUS-BBB opening on default mode network. A. Seed-based connectivity maps, B. difference maps in coronal planes and C. radar charts of resting state fMRI without FUS (baseline) and post-FUS (FUS only) and post-FUS with microbubbles (FUS + MB). With the seed selected in 8Ad of dlPFC (green crossed point in A), Default mode network nodes were found significantly activated after FUS and FUS-BBB opening compared to the baseline. The red-yellow and blue-light blue color maps indicate Fisher z-score maps with seeds in right 46d. L: left, R: right, A: anterior, P: posterior, S: superior, I: inferior.

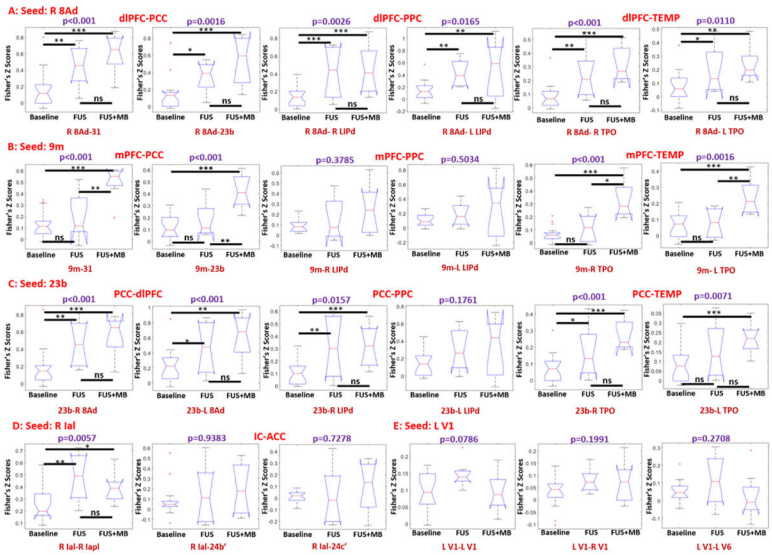

Fig. 6.

Seed-based correlation box plots with the seed ROI selected as right 8Ad (A), 9m (B), 23b(C), right Ial (D) and left V1 (E). The results indicated the changes in functional connectivity among dlPFC, PCC, PPC, TEMP, IC and ACC with the conditions of baseline, FUS and FUS with microbubbles (FUS + MB). The box plots showed the correlations of 25% percentile, 50% percentile, and 75% percentile, and outlining or extremely values. Statistical analysis was firstly performed using Kruskal-wallis test, with a purple $p < 0.05$ representing a significant difference. Post-hoc permutation test (5000 resamples) was performed when there was a significant difference among the three conditions, and × denotes $p < 0.05$, ** denotes $p < 0.01$, *** denotes $p < 0.001$ and ns denotes $p > 0.05$.

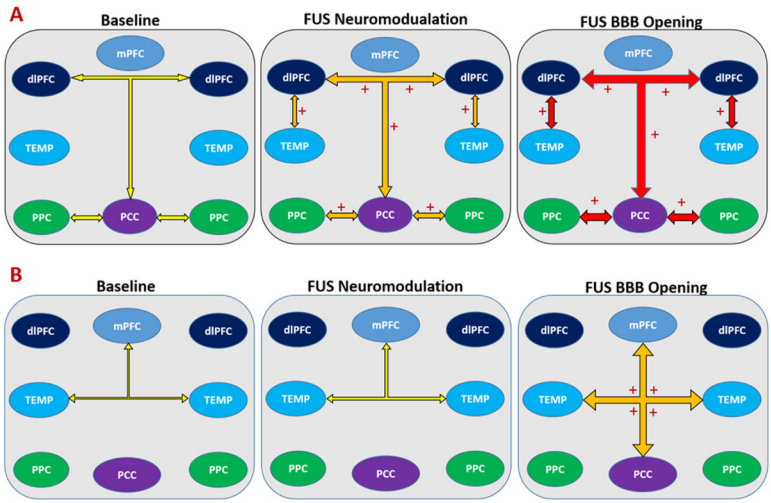

Fig. 7.

Summary of changes of functional connectivity on major brain networks among baseline, FUS neuromodulation and FUS-BBB opening. A. an activation of default mode network by both FUS neuromodulation and FUS-BBB opening; B. an activation of frontotemporal network by FUS-BBB opening. The width of arrow illustrates the average functional connectivity of the three conditions, with larger width indicating higher correlations. Colored arrow demonstrates the trend of changes on functional connectivity, with yellow, orange and red representing no change, modest and greatest magnitude changes compared to baseline respectively. + indicates a change (activation) with significant statistical difference compared to baseline.